CRYSTAL GROWTH & DESIGN

pubs.acs.org/crystal

Article

Halogen Bonding in Halothiophene Building Blocks

Published as part of Crystal Growth & Design virtual special issue "Lattice Dynamics".

Alisa Koivuporras, Aaron Mailman, Hongshuang Guo, Arri Priimagi,* and Rakesh Puttreddy*

Cite This: https://doi.org/10.1021/acs.cgd.3c00958

Read Online

ACCESS | Metrics & More | Article Recommendations | Supporting Information

ABSTRACT: Thiophenes bearing monotopic and symmetric ditopic halogen substituents and asymmetric ditopic halogen and pyridine substituents that act as halogen bond acceptors were evaluated for their halogen bonding interactions with 1,4-diiodotetrafluorobenzene and N-iodosuccinimide. The combinations resulted in C/N−I···X′ (X′ = Cl, Br, I) and C/N−I···N_{Py} (Py = pyridine) interactions, the former characterized by an interaction energy (ΔE_{int}) ranging from −4.4 to −18.7 kJ mol^{-1} and the latter from −26.3 to −56.0 kJ mol^{-1}. X-ray crystallography studies show that the ditopic asymmetric systems consisting of both halogens and pyridine self-associate through C−X···N_{Py} (X = Cl, Br, I) halogen bonding, and in their optimized structures the energies range from −5.4 to −19.6 kJ mol^{-1} depending on the type of halogen atom present. The ^{1}H NMR association constants of N−I···N_{Py} halogen bonds range between 1405 and 6397 M^{-1}. The σ-hole strengths of halogens have been useful in describing the interaction energies and solution models.

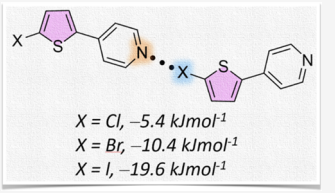

INTRODUCTION

Thiophene-based small molecules and polymers have gained a lot of attention as active components in organic electronics, owing to their wide range of attractive features including solution processability, tunable energy levels and absorption properties, high carrier mobility, and thermal stability.[1−3] These materials have been used in the development of a variety of devices, such as field-effect transistors,[4,5] sensors,[6] and photovoltaics.[7,8] Through theoretical and experimental research, it has been shown that even small alterations to the structure of thiophene lead to many noncovalent bonds, such as C−H···π and S···S interactions, which produce a highly aligned supramolecular architecture that affects charge-transfer mobility along the direction of the stacking.[3−5] This prompted the development of rational design principles that allow for the careful placement of functional groups onto thiophenes to produce energetically favourable molecular packings utilizing directional noncovalent interactions like hydrogen bonds and coordination bonds.[9] For example, the alkyl-urea-alkyl groups attached to thiophene and 2,2′-bisthiophene self-assemble into ribbon-like networks via N−H···O hydrogen bonds.[10] This causes the thiophene moieties to form a closely packed supramolecular network that provides an effective pathway for charge transport via π−π stacking. These hydrogen-bonded complexes have charge carrier mobilities (5×10^3 cm^2 V^{-1} s^{-1}) comparable to non-hydrogen-bonded polythiophene derivatives (7×10^3 cm^2 V^{-1} s^{-1}) whose packing is mostly stabilized by π−π interactions. In another instance, Bao et al. used Fe(III)-nitrogen coordination bonds to prepare metallo-supramolecular polymers based on diketopyrrolopyrrole-thiophene-pyridyl derivatives with field-effect mobilities of 2.2 cm^2 V^{-1} s^{-1}, which is two times higher than its parent polymer.[11] Despite remarkable advances in recent years that have resulted in the commercialization of devices, considerable efforts are still being made to improve their performance, stability, and functionality. Halogen bonding (XB),[12] a promising tool and more recent addition to the noncovalent interaction toolbox has gained a great deal of attention[13,14] as an equivalent and alternative to the ubiquitous hydrogen bonding.[15] Materials involving thiophenes as XB acceptors have been overlooked, with only a handful of halogen-bonded complexes investigated by Watkins et al.[16−18] and others.[19−24] It is important to further explore the use of XB-driven self-assembly of polythiophenes or other semiconducting polymers in organic electronics,[25] prior to which one must understand the interactions that dictate the assembly of corresponding small-molecule-based building blocks, which is the journey we embarked on in this work.

Halogen bonding is an attractive interaction of the type R−X···B, where X generally represents iodine or bromine and B can be any kind of Lewis base (N, O, S, etc.).[12] This interaction is based on the occurrence of a σ-hole, a region of lower electron density along the extension of an R−X bond arising from the anisotropic charge distribution around the X atom. Clark et al. explained this preference by performing natural bond order analysis on alkyl halides and proposing an approximate $s^2p_x^2p_y^2p_z^1$ configuration (where z is the direction

Received: August 10, 2023
Revised: October 27, 2023
Accepted: October 31, 2023

of the R−X bond) that explains head-on interactions of a halogen's electron-density-deficient site or σ-hole with nucleophiles.[26] As shown in Figure 1, pairing between the

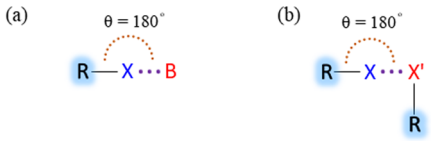

Figure 1. General representation of the XB interactions.

electron-rich region of one halogen substituent and the σ-hole of another halogen can also result in a R−X···X′−R (where X is a halogen and XB donor, X′ is a halogen and XB acceptor) type XB interaction.[27] In general, the XB strength decreases as the electronegativity of the halogen increases, i.e., in the order I > Br > Cl > F.[28] By including electron-withdrawing substituents, the σ-hole on the X atom can be enhanced, and such alterations lead to stronger XB interactions.[29] The very compact and electronegative fluorine atom only participates in XB under very specific conditions.[30] Because of the high directionality and broad range of tunable properties, there has been a rise in interest in halogen bonding studies in disciplines ranging from organic synthesis[31] to exert control over biological and polymeric assemblies.[32−34]

Here, we investigate the R−X···B and R−X···X′−R halogen bonding in 2-halothiophenes (**1**−**3**), 3-halothiophenes (**4**−**6**), 2,5-dihalothiophenes (**7**−**9**), and 5-(4-pyridyl)-2-halothiophenes (**10**−**12**) using 1,4-diiodotetrafluorobenzene (Dipfb) and *N*-iodosuccinimide (NIS) as XB donors. X-ray crystallography and solution NMR studies supported by computational calculations are used in tandem to explain our findings. Dipfb is a commonly used XB donor in materials chemistry,[33] however, since its iodine atoms are known to generate relatively weak XBs with both halogens and pyridine nitrogen, it is challenging to estimate (Dipfb)C−I···X/N binding in solution using NMR methods. As a result, for comparison purposes, NIS, which has strong electron-accepting iodine due to the presence of neighbouring C═O groups,[35] is utilized to evaluate the binding affinities of (NIS)N−I···X/N XB. We believe that this study will be helpful in the design and understanding of the intricate supramolecular interactions that help to design oligomeric and polymeric thiophenes and the functional materials that may arise from them (Figure 2).

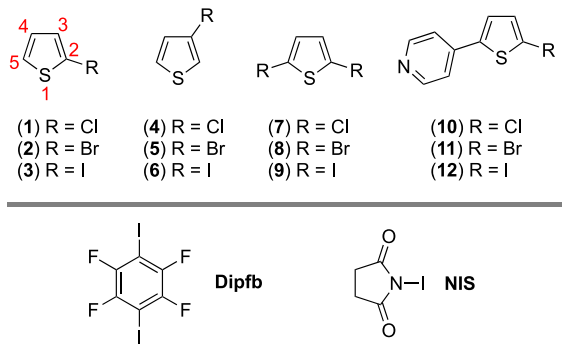

Figure 2. Chemical structures of thiophene XB acceptors (**1**−**12**) and XB donors, 1,4-diiodotetrafluorobenzene (Dipfb), and *N*-iodosuccinimide (NIS).

RESULTS AND DISCUSSION

DFT Computations. The evaluation of the local positive and negative electrostatic surface potentials of halogen and pyridinic nitrogen atoms is the first logical step in determining whether these molecules have the ability to form halogen bonds. The local positive electrostatic surface potential ($V_{s,max}$) of halogens and local negative electrostatic surface potential ($V_{s,min}$) of halogens as well as pyridyl nitrogen are computed at the PBE0-D3/def2-TZVP[36−42] level of theory to estimate the size of the halogen's σ-hole and electron belt, as well as the nitrogen atom's electron density. The iodine $V_{s,max}$ values are more positive than those of both bromine or chlorine, and they are in the expected order, I > Br > Cl (Figure 3 and Table S1).

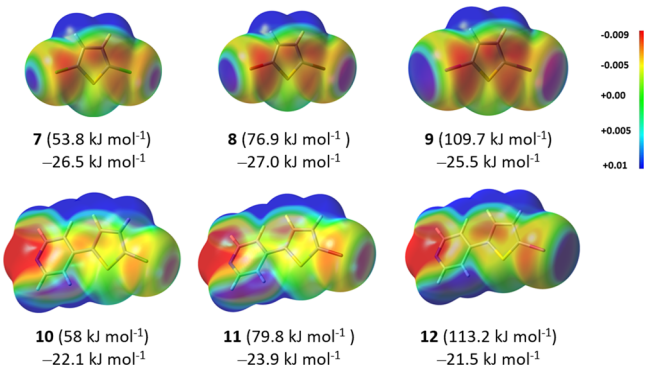

Figure 3. Computed electrostatic potential surface at the PBE0-D3/def2-TZVP level of theory projected on the 0.001 au electron density surfaces of halothiophenes (**7**−**12**) with $V_{s,max}$ (shown in parentheses) and $V_{s,min}$ values.

The σ-hole magnitude of the iodine in iodothiophenes (**3**, **6**, **9**, and **12**) varies between 97 and 113 kJ mol^{-1}, with the maximum of the range larger than commonly used iodine XB donors in crystal engineering studies, e.g., 1-iodoethynyl-4-iodobenzene (107 kJ mol^{-1}), 3,5-difluoro-1-iodobenzene (98 kJ mol^{-1}),[18] but smaller than Dipfb (>137 kJ mol^{-1}). The $V_{s,min}$ of C_5-pyridinic nitrogen in **10**−**12** is −147 to −148 kJ mol^{-1}, which suggests that their C_2-halogen atoms have little effect on the nitrogen $V_{s,min}$. On the other hand, the C_2-halogen atoms have the largest $V_{s,max}$ (and smallest $V_{s,min}$) values of any halothiophene derivative examined in the present study, implying that resonance effects and/or π-conjugation operate between the C_2-halogen and C_5-pyridine groups. The σ-hole strength of the C_2-halogen atom in the 2-halo, 2,5-dihalo, and 5-(4-pyridyl)-2-halothiophene series is influenced by the C_5-substituent. For instance, the C_5-group in the 2-chlorine series (**1**, **7**, and **10**) comprises hydrogen, chlorine, and the pyridyl ring, respectively. The decrease in C_2-chlorine $V_{s,max}$ values in the order **10** > **7** > **1** suggests that the electron-withdrawing propensity of the C_5-substituent decreases from the C_5-pyridyl to C_5-chlorine to hydrogen. The higher $V_{s,max}$ of C_2-chlorine in **10** may be attributed to effective π-delocalization caused by a larger π-surface area between the pyridine and thiophene systems.

Interaction energies (ΔE_{int}) were calculated in the gas phase, using the geometries obtained from single-crystal X-ray diffraction studies as the initial input for the geometry optimization, for the 1:1 halogen-bonded adducts formed by the donor and acceptor ligands (Figures 4a−c, S1−S4 and Table 1). All complexes demonstrate C/N−I···X′/N distances that are less than the sum of the van der Waals radii of the

https://doi.org/10.1021/acs.cgd.3c00958
Cryst. Growth Des. XXXX, XXX, XXX−XXX

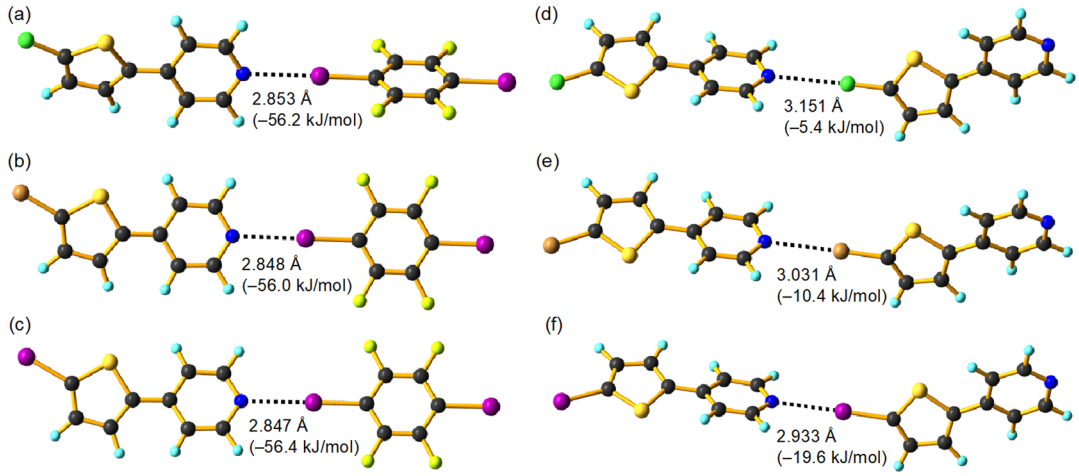

Figure 4. DFT-optimized halogen-bonded complexes of (a) Dipfb-**10**, (b) Dipfb-**11**, and (c) Dipfb-**12** and homodimers of **10**−**12**, (d) $\mathbf{10}_2$, (e) $\mathbf{11}_2$, and (f) $\mathbf{12}_2$. The black broken lines represent the XB interactions. Atom color code: carbon, black; nitrogen, blue; hydrogen, cyan; sulfur, yellow; fluorine, light green; chlorine, dark green; bromine, brown; purple, iodine.

Table 1. Interaction Energies Calculated at the PBE0-D3/def2-TZVP Level of Theory and ^{1}H NMR Association Constants (K_a M^{-1}, 293 K) for NIS Complexes in $CDCl_3$

complex[a]	ΔE_{int} (kJ mol^{-1})	complex	K_a, M^{-1} ($CDCl_3$)	ΔE_{int} (kJ mol^{-1})
Dipfb-**1**	−4.85	NIS-**1**	[a]	−9.67
Dipfb-**2**	−5.56	NIS-**2**	[a]	−12.3
Dipfb-**3**	−6.53	NIS-**3**	[a]	−16.69
Dipfb-**4**	−5.82	NIS-**4**	[a]	−11.59
Dipfb-**5**	−6.49	NIS-**5**	[a]	−14.35
Dipfb-**6**	−7.45	NIS-**6**	[a]	−18.7
Dipfb-**7**	−4.39	NIS-**7**	[a]	−8.95
Dipfb-**8**	−4.89	NIS-**8**	[a]	−11.46
Dipfb-**9**	−5.89	NIS-**9**	[a]	−15.77
Dipfb-**10**	−24.64	NIS-**10**	3188	−56.15
Dipfb-**11**	−25.31	NIS-**11**	6397	−55.94
Dipfb-**12**	−25.36	NIS-**12**	1405	−56.4

[a] K_a values estimation unsuccessful due to weak binding.

interacting atoms. The overall XB distances in Dipfb and NIS complexes range from 2.847 to 3.820 Å and 2.528 to 3.405 Å, respectively (see Table S2). The optimized C−I···N_{Py} distances of Dipfb-**10**−**12** complexes are 0.01−0.137 Å longer than XB contacts reported for cocrystals of iodoperfluorobenzenes and thiophene-bound pyridines,[16−18] which is to be expected given that crystal packing forces might have an impact on bond distances. Among the Dipfb complexes, the strongest XB interaction is observed for C−I···N_{Py} with −25 kJ mol^{-1}. The energies of C−I···X′−C (−4.4 to −7.5 kJ mol^{-1}) are small because the $V_{s,min}$ potentials of the halogen atoms are only modestly negative. The energies of the C−I···N_{Py} XB are smaller than those reported for C−I···N_{Py} formed by 1,3-difluoro/nitro-5-(iodoethynyl)benzene and 4-(5-(furan-2-yl)-thiophen-2-yl)pyridine, and 4-([2,2′-bithiophen]-5-yl)-pyridines.[18] We attribute this to the more electrophilic iodine in 1,3-difluoro/nitro-5-(iodoethynyl)benzene ($V_{s,max}$ > 156 kJ mol^{-1}) than the iodine atoms in Dipfb ($V_{s,max}$, 139 kJ mol^{-1}). The higher energies of iodoethynyl systems may also be attributed to stronger XB-accepting properties of the N_{Py}, whose nucleophilicity is enhanced by the larger π-system, enabling a tight overlap between the N_{Py} lone pair and the σ-hole of the halogen.[43] The interaction energy of C−I···N_{Py} XBs in 1:2 Dipfb:**10**−**12** trimer complexes was found to be −23.6 kJ mol^{-1}, which is ∼1 kJ mol^{-1} smaller than the interaction energy of the C−I···N_{Py} XBs in 1:1 Dipfb:**10**/**11**/**12** dimer complexes (for details, see Figure S5). The ΔE_{int}'s of N−I···X′−C in NIS-complex range from −8.9 to −16.7 kJ mol^{-1}, while those of N−I···N_{Py} are flat at −56 kJ mol^{-1}. Note the enhanced XB acceptor properties of the thiophene-bound halogen atoms with NIS iodine ($V_{s,max}$ 176 kJ mol^{-1}), which are reflected by their higher bond energies, suggesting that halogens are better XB acceptors in the presence of strong XB donors.

The C_5-pyridyl nitrogen and C_2-halogen in thiophenes **10**−**12** can form 1D chain-like structures via C−X···N_{Py} interactions. Not only would computing the bond energies of C−X···N_{Py} in homodimers help in the design and development of novel oligomeric and polymeric 4-pyridyl-halothiophene building blocks, but the influence of C_2-halogens on the XB acceptor properties of pyridinic nitrogen could be understood by comparing them to C−X···N_{Py} halogen bonds in Dipfb-**10**−**12**. From Figure 4, it is evident by comparing $\mathbf{10}_2$, $\mathbf{11}_2$, and $\mathbf{12}_2$ to Dipfb-**10**−**12** that the electronegativity of the passive C_2-halogens, meaning halogens that are not participating in XB, have no influence on the C−X···N_{Py} bond distances or energies, but they are only determined by the σ-hole strength of the XB-donating halogen. The C−I···N_{Py} distance of $\mathbf{12}_2$ (2.933 Å) is comparable to values reported for cocrystals, Dipfb-**12**, **9**·(4,4-bipyridine),[21] and **9**·(1,2-bis(2-pyridyl)-ethylene,[21] but it is about 0.160 Å shorter than, e.g., **9**·(phenazine)[21] and **9**·(tetramethylpyrazine).[21]

X-ray Crystallography. Only **9**−**12** and DIFTB-**11** yielded single crystals suitable for X-ray diffraction analysis, while attempts to crystallize ligands **1**−**8** and Dipfb/NIS complexes produced gel-like materials. Crystals of **9** belong to the orthorhombic space group *Pbca* with one molecule per asymmetric unit, which is consistent with a literature complex.[44] The C_2- and C_5-iodides function as XB donor and acceptor, and molecules of **9** self-associate through I···I interactions at distances of 3.721(5) Å (∠C−I···I′ = 174.2°) and 3.821(5) Å (∠C−I···I′ = 157.2°). These I···I distances have interaction energies of −2.0 and −3.6 kJ mol^{-1}, respectively, which are smaller than those of the I···I energies calculated for Dipfb- and NIS-iodothiophene complexes. In

https://doi.org/10.1021/acs.cgd.3c00958
Cryst. Growth Des. XXXX, XXX, XXX−XXX

addition, the thiophene rings are organized in an offset $\pi-\pi$ stacking mode with a short contact of 3.95 Å between the centroid of the thiophene ring and the iodine substituent (Figure S6). These additional interactions contribute to the assembly's stability. In all three **10**−**12** structures, the thiophenes form 1D chains via C−X···N_{Py} halogen bonds at distances of 3.075(2) Å (∠C−Cl···N = 168.3°; **10**), 3.007(2) Å (∠C−Br···N = 169°; **11**), and 2.862(3) Å (∠C−I···N = 176.4°; **12**) that are less than the sum of the van der Waals radii of the corresponding interacting atoms (Cl + N = 3.30 Å; Br + N = 3.40 Å; I + N = 3.53 Å;[45] Figure 5). There is no $\pi-\pi$ stacking in **10**−**12**; instead, these molecules are stabilized via C−H··· π interactions (ca. 2.80−2.98 Å) between pyridine and thiophene rings as shown in Figure S7. The cocrystal Dipfb-**11** crystallizes in the triclinic space group *P*-1 (No. 2) and its asymmetric unit contains one molecule of **11** and half a molecule of Dipfb (see Figure S9, for PXRD data). The overall stoichiometry is two XB acceptors per Dipfb. Each Dipfb molecule forms a C−I···N_{Py} XB via iodine to a nitrogen on **11**. The bond is characterized by an I···N distance of 2.800(3) Å (∠C−I···N = 174.6°). Each Dipfb molecule further forms an unexpected XB via one of its fluorine atoms with the bromine of **11** at distances of 3.222(2) Å (∠C−Br···F = 163.3°). These C−Br···F halogen bonds are probably the result of packing forces, yet they are essential for stabilizing the crystals. In contrast to **10**−**12**, the presence of Dipfb contributes to the observation of two distinctive π-stacking interactions between two Dipfb molecules at distances of 3.66−3.98 Å and two thiophene molecules at a distance of 3.98 Å. It should be noted that, although XB and $\pi-\pi$ stacking plays the most competitive role in the crystal structures, several Dipfb-related secondary interactions, including F···H and F···C (Figure S8), were observed in Dipfb-**11** due to the Dipfb's tendency to generate F- and π-centered contacts.[46]

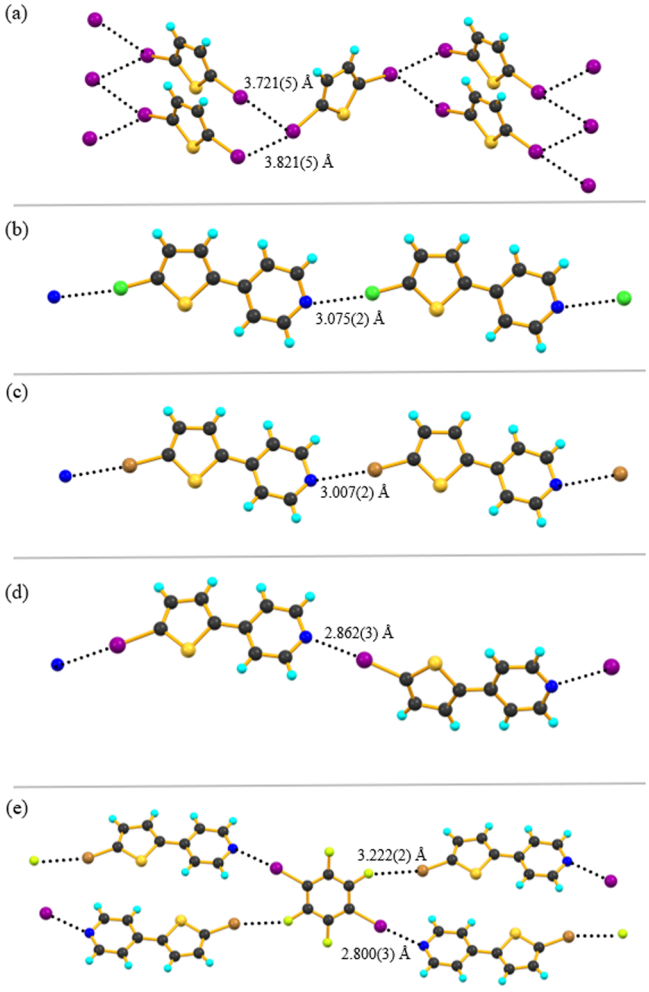

Figure 5. Partial polymeric halogen-bonded chain view of (a) **9**, (b) **10**, (c) **11**, (d) **12**, and (e) Dipfb-**11**. The black dotted lines represent halogen bonding interactions.

Packing analysis of **10**−**12** reveals that adjacent 1D chains are interconnected to form a 2D layer via other noncovalent interactions such as C−H···π and C−H···N. We performed Hirshfeld surface (HS) analysis[47−49] to gain a deeper understanding of the different noncovalent interactions, particularly the non-halogen-based intermolecular interactions, that are present in crystals **10**−**12**. This information is crucial, especially when designing and developing oligomeric and polymeric thiophenes containing halogen and pyridyl groups and identifying which noncovalent interactions are key to stabilizing the molecules and the bulk. The HS analysis is a valuable tool for quantifying intermolecular interactions in crystal molecular packing. The parameters mapped onto the HS are d_e and d_i, which are defined as the distances from the surface to the nearest atom exterior and internal to the created HS. A d_{norm} mapped HS is produced by adding their normalized d_e and d_i values to the respective atoms' van der Waals radii. Red spots appear on a norm surface when the distance between the contact atoms is less than the sum of their van der Waals radii. Contacts that are closer to or near van der Waals radii are white, while longer contacts have a blue contour. Figure 6 depicts an example of the d_{norm} surface of ligand **10**. A d_e and d_i 2D plot using the HS describes quantitatively the nature and type of noncovalent contacts in crystals.

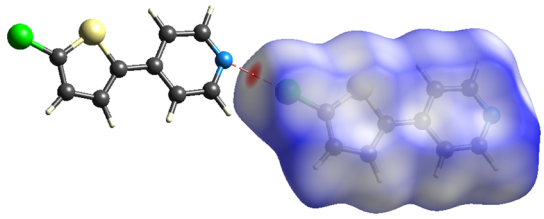

Figure 6. Ball-and-stick model and a Hirshfeld surface of **10** mapped over d_{norm} (on the right side) in the range −0.1372 and +1.0679 au displaying C−Cl···N interaction (the red-hot spot). The surface is generated by using the software CrystalExplorer.[50] Atom color code: carbon, black; nitrogen, blue; hydrogen,white; sulfur, yellow; chlorine, dark green.

The distribution of the average of individual intermolecular interactions in the three ligands is shown by the pie chart in Figure 7. The HS analysis reveals that in the molecular packing, the role of hydrogen-centered intermolecular interactions is prominent. The highest proportion of C···H interactions that are a measure of C−H···π contacts were observed, constituting 24.7% of the surfaces. The analysis shows high contributions of attractive intermolecular H···H contacts (18.1%), which agrees with the volume of H atoms present on the ligand backbone. The overall S···H and N···H interactions each contribute only 10.4 and 7.7% to the surfaces, yet these directional hydrogen bonds act in concert to

https://doi.org/10.1021/acs.cgd.3c00958
Cryst. Growth Des. XXXX, XXX, XXX−XXX

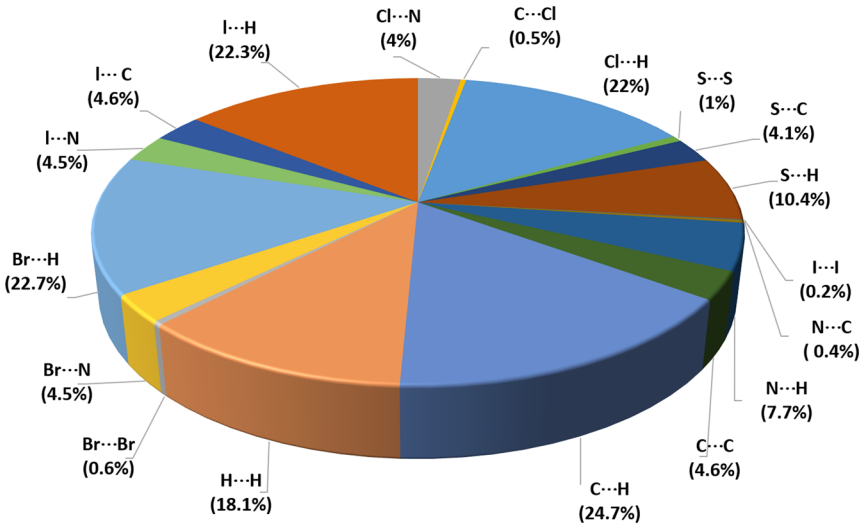

Figure 7. Distribution of the average of the individual intermolecular interactions in **10**−**12** crystal structures.

minimize the global electrostatic repulsions of molecules in crystals. The electron-deficient sulfur atoms have areas of positive and negative electrostatic potentials that are available for attractive interactions with nucleophiles and electrophiles. It implies that σ-hole bonding can occur between identical molecules via the same atom (e.g., S···S), with the σ-hole on one sulfur interacting with a negative region (e.g., S···I) on the other, as shown in Figure S6. Note that the position and number of sulfur atoms in thiophenes play an important role in molecular π-conjugation, the formation and strength of sulfur intermolecular contacts, and the performance of devices, and this has attracted a lot of attention in engineering thiophene building blocks in the field of organic electronics.[51,52] In haloaryl compounds **10**−**12**, the negative electron belt orthogonal to the σ-hole of C−X bonds considerably demands X···H (22% in **10**, 22.7% in **11**, and 22.3% in **12**) and I···C (4.6%) interactions as structure-directing motifs, whereas the lowest contributions of Cl/Br···C (<0.6%) and I···I (<0.2%) imply that these are merely an outcome of packing factors. In addition, the C···C contacts (4.6%), a measure of π−π interactions, are observed between thiophene and pyridyl rings. Contributions associated with the XB are Cl···N (4%), Br···N (4.5%), and I···N (4.5%), N···C (2%), and O···N (1%).

Solution NMR. Considering the computed interaction energies as well as the presence of halogen substituents and pyridinic nitrogen atoms in **10**−**12**, we hypothesized that when combined with Dipfb/NIS, C/N−I···X′/N_{Py} (X′ = Cl, Br, I), XBs might be detectable in solution. To verify this, ^{1}H NMR spectroscopy was used to examine a 1:1 equiv mixture of Dipfb and **3** in $CDCl_3$. Unfortunately, the chemical shifts of Dipfb:**3** and pure **3** were identical, indicating no XB. Similar behavior was seen with a 1:1 mixture of NIS and **3**, where the protons from NIS $-CH_2-$ showed the same chemical shift as the pure NIS. The test results indicate that the X′/N-acceptor of (Dipfb)C−I···X′/N and (NIS)N−I···X′ is too weak to allow significant binding, even in the XB non-competitive solvent $CDCl_3$. In the cases of (Dipfb)C−I···X′ and (NIS)N−I···X′, we can also attribute this to the weak electron-donating power of thiophene-bound halogens, and this is reflected by their nearly similar $V_{s,min}$ values (the maximum difference between $V_{s,min}$ of the halogen atoms was 3.5 kJ mol^{-1} for 2-halo, 4.7 kJ mol^{-1} for 3-halo-, 1.5 kJ mol^{-1} for 2,5-dihalo-, and 2.4 kJ mol^{-1} for the 5-halo-2-pyridyl series).

Large chemical shift differences were found for NIS protons in complexes of NIS-**10**−**12** when compared to pure NIS $-CH_2-$ signals, confirming the XB complexation in solution. The NIS methylene chemical shift changes were used to assess the N−I···N_{Py} interactions (Figures S5−S7). K_a values were calculated using the online Bindfit tool.[53] The experimental K_a values of NIS-**10**, NIS-**11**, and NIS-**12** were 3188, 6397, and 1405 M^{-1}, respectively, and they demonstrated a 1:1 fitting binding model. In NIS-**10**−**12**, it is clear that the pyridinic nitrogen atoms interacted with the NIS donor because the ^{1}H NMR test results of NIS-**3** did not show any chemical shift changes. The modest electron-donating capacity of C_5-halogens makes the N−I···X′−C halogen−halogen interactions in this presumed 1:1 solution model appear insignificant. Based on solution NMR and DFT data, we hypothesize that the $V_{s,min}$ of thiophene-bound halogen atoms should be near to the $V_{s,min}$ of C_5-pyridyl nitrogen, or that the $V_{s,max}$ of thiophene-bound halogen atoms should be higher than the $V_{s,max}$ of NIS to obtain K_a values for C/N−I···X′−C XBs using NMR methods.

CONCLUSIONS

In conclusion, halogenothiophenes and pyridylhalothiophenes interact with Dipfb and NIS XB donors, forming C/N−I···X′/N_{Py} (X′ = Cl, Br, I) XB interactions. Computational results demonstrate that thiophene-bound halogen atoms are good XB acceptors and donors. In the latter case, the σ-hole potentials are comparable to those of commonly used iodo- and bromoethynyl XB donors. Interaction energies of C/N−I···X′ and C/N−I···N_{Py} XBs are in the −4.4 to −18.7 kJ mol^{-1} and −26.3 to −56.0 kJ mol^{-1} range, respectively. X-ray crystallographic analysis of 5-(4-pyridyl)-2-halothiophenes suggests that their 1D polymeric chain assemblies are driven by intermolecular C−X···N halogen bonds and energetically competitive C−H···π noncovalent interactions, whereas in the cocrystal formed between 1,4-diiodotetrafluorobenzene and 5-(4-pyridyl)-2-bromothiophene by XB and π-stacking. This observation suggests that (i) the technique of having XB donor and acceptor atoms on a thiophene structure and XB-mediated self-assembly in their native state, as demonstrated using **10**−**12**, can be applied to prepare oligo- and

https://doi.org/10.1021/acs.cgd.3c00958
Cryst. Growth Des. XXXX, XXX, XXX−XXX

polythiophene-based conductive π-conjugative polymers, and (ii) in the cocrystal case, numerous types of noncovalent bonds coexist, with all fluorine atoms of the Dipfb involved, implying that XBs and fluorine can work together and exert a distinct level of control over the supramolecular structure, demonstrating their role as structure-directing components for designing functional materials. HS analysis was applied on halopyridylthiophenes to quantify numerous noncovalent connections that are not immediately apparent from the molecular packing structures. Through this study, a high distribution of H-centered interactions (>70%) represents structure-directing interactions in addition to C−X···N halogen bonds. In solution, the C/N−I···X′ XBs are too weak to be measured with ^{1}H NMR spectroscopy. Yet association constants of N−I···N_{Py} XBs as large as 6697 M^{-1} could be obtained for three complexes. This systematic study provides experimental and theoretical data that can serve as fundamental knowledge while designing thiophene-based materials for applications in organic electronics.

EXPERIMENTAL SECTION

General Information. All solvents used for synthesis and crystallizations are HPLC grade and used as received. Chloroform-d_6 was purchased from Acros Organics. 2-Chlorothiophene (**1**), 2-bromothiophene (**2**), 2-iodothiophene (**3**), 3-chlorothiophene (**4**), 3-bromothiophene (**5**), 3-iodothiophene (**6**), 2,5-dichlorothiophene (**7**), 2,5-dibromothiophene (**8**), 2,5-diiodothiophene (**9**), and N-iodosuccinimide (NIS) were purchased from TCI Chemicals Europe, and 1,4-diiodotetrafluorobenzene (Dipfb) from Apollo Scientifics. 2-Chloro-5-(4-pyridyl)thiophene (**10**), 2-bromo-5-(4-pyridyl)-thiophene (**11**), and 2-iodo-5-(4-pyridyl)thiophene (**12**) were synthesized following the literature procedure. Infrared spectra of **10**−**12** were recorded using Bruker Tensor 27 FTIR spectrometer, attenuated total reflection (ATR) mode (See Supporting Information Figures S11−S18). Melting points of **10**−**12** are obtained using Stuart SMP10.

X-ray Crystallography. Single-crystal X-ray data of **9**−**12** were measured using Rigaku SuperNova dual-source Oxford diffractometer equipped with an Atlas detector employing mirror-monochromated Cu-$K\alpha$ (λ = 1.54184 Å) radiation, whereas Dipfb-**11** was collected using single-source Rigaku SuperNova diffractometer equipped with an Atlas or Eos CCD detector using mirror-monochromated Mo−$K\alpha$ radiation (λ = 0.71073 Å). The data collection and reduction are performed by using the *CrysAlisPro*.[54] The structure is solved with direct methods (*SHELXS*)[55] and refined by full-matrix least-squares on F^2 using the *OLEX2* software,[56] which utilizes the *SHELXL*-2014 module.[57] The single-crystal X-ray data, experimental details, and CCDC numbers (2286686−2286690) are given below.

Crystal data of **9**: CCDC-2286687, $C_4H_2I_2S$, M = 335.92 g mol^{-1}, colorless block, 0.048 × 0.042 × 0.036 mm^3, orthorhombic, space group *Pbca* (No. 61), a = 5.2377(3) Å, b = 14.9290(7) Å, c = 18.2311(8) Å, α = 90°, β = 90°, γ = 90°, V = 1425.56(12) Å^3, Z = 8, D_{calc} = 3.130 g cm^3, F(000) = 1184, μ = 71.119 mm^{-1}, T = 120 K, θ_{max} = 76.57°, 4723 total reflections, 1324 with $I_o > 2\sigma$(Io), R_{int} = 0.0366, 1483 data, 64 parameters, 0 restraints, GooF = 1.066, R_1 = 0.0266 and wR_2 = 0.0630 [$I_o > 2\sigma(I_o)$], R_1 = 0.0315 and wR_2 = 0.0653 (all reflections), 0.764 < d$\Delta\rho$ < − 0.937 eÅ^3.

Crystal data of **10**: CCDC-2286686, C_9H_6ClNS, M = 195.66 g mol^{-1}, colorless block, 0.157 × 0.127 × 0.055 mm^3, monoclinic, space group $P2_1/c$ (No. 14), a = 9.7481(2) Å, b = 14.3783(3) Å, c = 5.86700(10) Å, α = 90°, β = 91.712(2)°, γ = 90°, V = 821.96(3) Å^3, Z = 4, D_{calc} = 1.581 g cm^3, F(000) = 400, μ = 5.935 mm^{-1}, T = 120 K, θ_{max} = 76.917°, 5334 total reflections, 1594 with $I_o > 2\sigma(I_o)$, R_{int} = 0.0260, 1729 data, 109 parameters, 0 restraints, GooF = 1.051, R_1 = 0.0269 and wR_2 = 0.0300 [$I_o > 2\sigma(I_o)$], R_1 = 0.0679 and $wR2$ = 0.0716 (all reflections), 0.346< d$\Delta\rho$ < −0.326 eÅ^3.

Crystal data of **11**: CCDC-2286689, C_9H_6BrNS, M = 240.12 g mol^{-1}, colorless plate, 0.197 × 0.114 × 0.043 mm^3, monoclinic, space group $P2_1/c$ (No. 14), a = 9.8689(2) Å, b = 14.4105(3) Å, c = 5.97100(10) Å, α = 90°, β = 91.990(2)°, γ = 90°, V = 848.66(3) Å^3, Z = 4, D_{calc} = 1.879 g cm^3, F(000) = 472, μ = 8.369 mm^{-1}, T = 120 K, θ_{max} = 76.706°, 5254 total reflections, 1649 with $I_o > 2\sigma(I_o)$, R_{int} = 0.0205, 1757 data, 109 parameters, 0 restraints, GooF = 1.064, R_1 = 0.0200 and wR_2 = 0.0510 [$I_o > 2\sigma(I_o)$], R_1 = 0.0220 and wR_2 = 0.0525 (all reflections), 0.315 < d$\Delta\rho$ < −0.444 eÅ^3.

Crystal data of **12**: CCDC-2286690, C_9H_6INS, M = 287.11 g mol^{-1}, colorless block, 0.162 × 0.141 × 0.069 mm^3, monoclinic, space group $P2_1/c$ (No. 14), a = 11.0797(5) Å, b = 5.5556(2)Å, c = 15.6908(7) Å, α = 90°, β = 109.218(5)°, γ = 90°, V = 912.01(7) Å^3, Z = 4, D_{calc} = 2.091 g cm^3, F(000) = 544, μ = 29.235 mm^{-1}, T = 120 K, θ_{max} = 76.664°, 5598 total reflections, 1698 with $I_o > 2\sigma(I_o)$, R_{int} = 0.0348, 1861 data, 109 parameters, 0 restraints, GooF = 1.058, R_1 = 0.0319 and wR_2 = 0.0838 [$I_o > 2\sigma(I_o)$], R_1 = 0.0351 and wR_2 = 0.0883 (all reflections), 1.500 < d$\Delta\rho$ < −1.071eÅ^3.

Crystal data of DIPFB-**11**: CCDC-2286688, $C_{24}H_{12}Br_2F_4I_2N_2S_2$, M = 882.10 g mol^{-1}, colorless block, 0.191 × 0.093 × 0.053 mm^3, triclinic, space group P-1 (No. 2), a = 3.9836(2) Å, b = 12.3590(4)Å, c = 13.3035(6)Å, α = 94.712(3)°, β = 90.150(3)°, γ = 95.438(3)°, V = 649.79(5) Å^3, Z = 8, D_{calc} = 2.254 g cm^3, F(000) = 414, μ = 5.702 mm^{-1}, T = 120 K, θ_{max} = 29.676°, 4896 total reflections, 2856 with $I_o > 2\sigma(I_o)$, R_{int} = 0.0237, 3134 data, 163 parameters, 0 restraints, GooF = 1.093, R_1 = 0.0290 and wR_2 = 0.0572 [$I_o > 2\sigma(I_o)$], R_1 = 0.0344 and wR_2 = 0.0626 (all reflections), 0.893 < d$\Delta\rho$ < −0.788 eÅ^3.

Synthesis of 5-Halo-2-(4-pyridyl)thiophenes. 5-Chloro-2-(4-pyridyl)thiophene (**10**): This compound was synthesized as described previously.[58] Mp: 119−121 °C; ^{1}H NMR [500 MHz, $CDCl_3$]: δ = 8.58 (d, J = 4.8 Hz), 7.37 (d, J = 6.2 Hz), 7.28 (d, J = 4.0 Hz), 6.94 (d, J = 4.0 Hz); ^{13}C NMR [125 MHz, $CDCl_3$]: δ = 150.28, 140.92, 139.48, 132.30, 127.75, 124.96, 119.51; MS calcd for C_9H_6ClNS 194.99822, found 196.00120; ATR-FTIR ν_{max} = 3073, 3032, 2981,1932, 1774, 1588, 1549, 1483, 1432, 1412, 1314, 1257, 1218, 1064, 1015, 988, 962, 889, 859, 802, 730, 710, 694, 663, 642, 611 cm^{-1}.

5-Bromo-2-(4-pyridyl)thiophene (**11**): This compound was synthesized following the literature procedure.[59] Mp: 156−158 °C; ^{1}H NMR (500 MHz, $CDCl_3$): δ = 8.59 (s), 7.38 (d, J = 5.6 Hz), 7.26−7.23 (m), 7.08 (d, J = 3.8 Hz); ^{13}C NMR (125 MHz, $CDCl_3$): δ = 159.29, 142.43, 140.84, 131.46, 125.84, 119.66, 119.61, 114.73; MS calcd for C_9H_6BrNS 239.94771, found 239.94794; ATR-FTIR ν_{max} = 3075, 3031, 2982, 1933, 1774, 1589, 1548, 1484, 1425, 1412, 1312, 1220, 1070, 1061, 993, 983, 952, 889, 860, 799, 730, 693, 663, 630 cm^{-1}.

5-Iodo-2-(4-pyridyl)thiophene (**12**): This compound was synthesized using literature method.[58] Mp: 210−212 °C; ^{1}H NMR (500 MHz, $CDCl_3$): δ = 8.58 (d, J = 5.4 Hz), 7.39 (dd, J = 4.6, 1.6 Hz), 7.27 (d, J = 3.9 Hz), 7.16 (d, J = 3.8 Hz); ^{13}C NMR (125 MHz, $CDCl_3$): δ = 150.34, 146.96, 140.63, 138.43, 126.91, 119.73; MS calcd for C_9H_6INS 287.93384, found 287.93452; ATR-FTIR ν_{max} = 3091, 3024, 2921, 1940, 1762, 1640, 1588, 1546, 1527, 1484, 1415, 1309, 1219, 1091, 1056, 995, 972, 956, 932, 863, 818, 789, 727, 696, 660, 627 cm^{-1}.

ASSOCIATED CONTENT

Supporting Information

The Supporting Information is available free of charge at https://pubs.acs.org/doi/10.1021/acs.cgd.3c00958.

DFT computational, NMR, and X-ray crystallographic data (PDF)

Accession Codes

CCDC 2286686−2286690 contain the supplementary crystallographic data for this paper. These data can be obtained free of charge via www.ccdc.cam.ac.uk/data_request/cif, or by emailing data_request@ccdc.cam.ac.uk, or by contacting The

https://doi.org/10.1021/acs.cgd.3c00958
Cryst. Growth Des. XXXX, XXX, XXX−XXX

Cambridge Crystallographic Data Centre, 12 Union Road, Cambridge CB2 1EZ, UK; fax: +44 1223 336033.

AUTHOR INFORMATION

Corresponding Authors

Arri Priimagi − *Department of Chemistry, University of Jyvaskyla, Jyvaskyla FI-40014, Finland;* orcid.org/0000-0002-5945-9671; Email: arri.priimagi@tuni.fi

Rakesh Puttreddy − *Smart Photonic Materials, Faculty of Engineering and Natural Sciences, Tampere University, Tampere FI-33720, Finland; Department of Chemistry, University of Jyvaskyla, Jyvaskyla FI-40014, Finland;* Email: rakesh.r.puttreddy@jyu.fi

Authors

Alisa Koivuporras − *Smart Photonic Materials, Faculty of Engineering and Natural Sciences, Tampere University, Tampere FI-33720, Finland*

Aaron Mailman − *Department of Chemistry, University of Jyvaskyla, Jyvaskyla FI-40014, Finland;* orcid.org/0000-0003-2067-8479

Hongshuang Guo − *Department of Chemistry, University of Jyvaskyla, Jyvaskyla FI-40014, Finland;* orcid.org/0000-0003-3503-1774

Complete contact information is available at: https://pubs.acs.org/10.1021/acs.cgd.3c00958

Notes

The authors declare no competing financial interest.

ACKNOWLEDGMENTS

The authors gratefully acknowledge financial support from the Academy of Finland (SUPREL project, No. 326416 for A.P. and Postdoctoral Fellowship, No. 347201, for H.G.). The work is conducted as part of the Academy of Finland Center of Excellence Programme LIBER, No. 346107 and the Flagship Programme PREIN, No. 320165. We thank Shreya Mahajan for her assistance with the PXRD.

REFERENCES

(1) Perepichka, I. F.; Perepichka, D. F. *Handbook of Thiophene Based Materials*. 2009, John Wiley & Sons: Chichester, DOI: DOI: 10.1002/9780470745533.

(2) Liu, K.; Ouyang, B.; Guo, X.; Guo, Y.; Liu, Y. Advances in Flexible Organic Field-Effect Transistors and Their Applications for Flexible Electronics. *npj Flexible Electron.* **2022**, *6* (1), 1.

(3) Cinar, M. E.; Ozturk, T. Thienothiophenes, Dithienothiophenes, and Thienoacenes: Syntheses, Oligomers, Polymers, and Properties. *Chem. Rev.* **2015**, *115* (9), 3036−3140.

(4) Wu, W.; Liu, Y.; Zhu, D. π-Conjugated Molecules with Fused Rings for Organic Field-Effect Transistors: Design, Synthesis and Applications. *Chem. Soc. Rev.* **2010**, *39* (5), 1489−1502.

(5) Zhang, L.; Di, C.; Yu, G.; Liu, Y. Solution Processed Organic Field-Effect Transistors and Their Application in Printed Logic Circuits. *J. Mater. Chem.* **2010**, *20* (34), 7059−7073.

(6) Fernandes, R. S.; Shetty, N. S.; Mahesha, P.; Gaonkar, S. L. A Comprehensive Review on Thiophene Based Chemosensors. *J. Fluoresc.* **2022**, *32* (1), 19−56.

(7) Zheng, B.; Huo, L.; Li, Y. Benzodithiophenedione-Based Polymers: Recent Advances in Organic Photovoltaics. *NPG Asia Mater.* **2020**, *12* (1), 3.

(8) Mehmood, U.; Al-Ahmed, A.; Hussein, I. A. Review on Recent Advances in Polythiophene Based Photovoltaic Devices. *Renewable Sustainable Energy Rev.* **2016**, *57*, 550−561.

(9) Ravva, M. K.; Risko, C.; Brédas, J. L. Noncovalent Interactions in Organic Electronic Materials. In *Non-Covalent Interactions in Quantum Chemistry and Physics: Theory and Applications*; Elsevier Inc., 2017; pp 277−302.

(10) Schoonbeek, F. S.; Van Esch, J. H.; Wegewijs, B.; Rep, D. B. A.; De Haas, M. P.; Klapwijk, T. M.; Kellogg, R. M.; Feringa, B. L. Efficient Intermolecular Charge Transport in Self-Assembled Fibers of Mono- and Bithiophene Bisurea Compounds. *Angew. Chem., Int. Ed.* **1999**, *38* (10), 1393−1397.

(11) Wu, H. C.; Lissel, F.; Wang, G. J. N.; Koshy, D. M.; Nikzad, S.; Yan, H.; Xu, J.; Luo, S.; Matsuhisa, N.; Cheng, Y.; Wang, F.; Ji, B.; Li, D.; Chen, W. C.; Xue, G.; Bao, Z. Metal−Ligand Based Mechanophores Enhance Both Mechanical Robustness and Electronic Performance of Polymer Semiconductors. *Adv. Funct. Mater.* **2021**, *31* (11), No. 2009201.

(12) Desiraju, G. R.; Shing Ho, P.; Kloo, L.; Legon, A. C.; Marquardt, R.; Metrangolo, P.; Politzer, P.; Resnati, G.; Rissanen, K. Definition of the Halogen Bond (IUPAC Recommendations. *Pure Appl. Chem.* **2013**, *2013*, 1711−1713.

(13) Priimagi, A.; Cavallo, G.; Metrangolo, P.; Resnati, G. The Halogen Bond in the Design of Functional Supramolecular Materials: Recent Advances. *Acc. Chem. Res.* **2013**, *46* (11), 2686−2695.

(14) Lim, J. Y. C.; Beer, P. D. Sigma-Hole Interactions in Anion Recognition. *Chem* **2018**, *4* (4), 731−783.

(15) Arunan, E.; Desiraju, G. R.; Klein, R. A.; Sadlej, J.; Scheiner, S.; Alkorta, I.; Clary, D. C.; Crabtree, R. H.; Dannenber, J. J.; Hobza, P.; Kjaergaard, H. G.; Legon, A. C.; Mennucci, B.; Nesbitt, D. J. Definition of the Hydrogen Bond (IUPAC Recommendations 2011). *Pure Appl. Chem.* **2011**, *83* (8), 1637−1641.

(16) Wilson, J.; Dal Williams, J. S.; Petkovsek, C.; Reves, P.; Jurss, J. W.; Hammer, N. I.; Tschumper, G. S.; Watkins, D. L. Synergistic Effects of Halogen Bond and π-π Interactions in Thiophene-Based Building Blocks. *RSC Adv.* **2015**, *5* (100), 82544−82548.

(17) Johnson, S. N.; Ellington, T. L.; Ngo, D. T.; Nevarez, J. L.; Sparks, N.; Rheingold, A. L.; Watkins, D. L.; Tschumper, G. S. Probing Non-Covalent Interactions Driving Molecular Assembly in Organo-Electronic Building Blocks. *CrystEngComm* **2019**, *21* (20), 3151−3157.

(18) Nguyen, S. T.; Ellington, T. L.; Allen, K. E.; Gorden, J. D.; Rheingold, A. L.; Tschumper, G. S.; Hammer, N. I.; Watkins, D. L. Systematic Experimental and Computational Studies of Substitution and Hybridization Effects in Solid-State Halogen Bonded Assemblies. *Cryst. Growth Des.* **2018**, *18* (5), 3244−3254.

(19) Berger, G.; Soubhye, J.; van der Lee, A.; Vande Velde, C.; Wintjens, R.; Dubois, P.; Clément, S.; Meyer, F. Interplay between Halogen Bonding and Lone Pair−π Interactions: A Computational and Crystal Packing Study. *ChemPlusChem* **2014**, *79* (4), 552−558.

(20) Kumar, S.; Body, C.; Leyssens, T.; Van Hecke, K.; Berger, G.; Van der Lee, A.; Laurencin, D.; Richeter, S.; Clément, S.; Meyer, F. Halogen-Bonded Thiophene Derivatives Prepared by Solution and/or Mechanochemical Synthesis. Evidence of N···S Chalcogen Bonds in Homo- and Cocrystals. *Cryst. Growth Des.* **2023**, *23* (4), 2442−2454.

(21) Ragusa, A. C.; Peloquin, A. J.; McMillen, C. D.; Pennington, W. T. 2,5-Diiodothiophene: A Versatile Halogen Bonding Synthon for Crystal Engineering. *Cryst. Growth Des.* **2022**, *22* (3), 1906−1913.

(22) Patra, A.; Wijsboom, Y. H.; Leitus, G.; Bendikov, M. Tuning the Band Gap of Low-Band-Gap Polyselenophenes and Polythiophenes: The Effect of the Heteroatom. *Chem. Mater.* **2011**, *23* (3), 896−906.

(23) Baykov, S. V.; Presnukhina, S. I.; Novikov, A. S.; Shetnev, A. A.; Boyarskiy, V. P.; Kukushkin, V. Yu. 2,5-Dibromothiophenes: Halogen Bond Involving Packing Patterns and Their Relevance to Solid-State Polymerization. *Cryst. Growth Des.* **2021**, *21* (4), 2526−2540.

(24) Mamon, Sereda Akash; Anwar, Hussain; Zefirov Nikolai, G. S. Solvent-Free and Liquid-Phase Iodination of Thiophene Derivatives with Potassium Dichloroiodate Monohydrate. *Synthesis* **2020**, *52* (07), 1140−1146.

(25) Bocheux, A.; Tahar-Djebbar, I.; Fiorini-Debuisschert, C.; Douillard, L.; Mathevet, F.; Attias, A.-J.; Charra, F. Self-Templating

Polythiophene Derivatives: Electronic Decoupling of Conjugated Strands through Staggered Packing. *Langmuir* **2011**, *27* (16), 10251−10255.
(26) Clark, T.; Heßelmann, A. The Coulombic σ-Hole Model Describes Bonding in $CX_3I\cdots Y^-$ Complexes Completely. *Phys. Chem. Chem. Phys.* **2018**, *20* (35), 22849−22855.
(27) Scheiner, S. Characterization of Type I and II Interactions between Halogen Atoms. *Cryst. Growth Des.* **2022**, *22* (4), 2692−2702.
(28) Clark, T.; Hennemann, M.; Murray, J. S.; Politzer, P. Halogen Bonding: The σ-Hole. *J. Mol. Model.* **2007**, *13* (2), 291−296.
(29) Wolters, L. P.; Schyman, P.; Pavan, M. J.; Jorgensen, W. L.; Bickelhaupt, F. M.; Kozuch, S. The Many Faces of Halogen Bonding: A Review of Theoretical Models and Methods. *Wiley Interdiscip. Rev. Comput. Mol. Sci.* **2014**, *4* (6), 523−540.
(30) Eskandari, K.; Lesani, M. Does Fluorine Participate in Halogen Bonding? *Chem − Eur. J.* **2015**, *21* (12), 4739−4746.
(31) Schindler, S.; Huber, S. M. Halogen Bonds in Organic Synthesis and Organocatalysis. In *Halogen Bonding II: Impact on Materials Chemistry and Life Sciences*; Metrangolo, P.; Resnati, G., Eds.; Springer International Publishing: Cham, 2015; pp 167−203.
(32) Scholfield, M. R.; Zanden, C. M.; Vander; Carter, M.; Ho, P. S. Halogen Bonding (X-Bonding): A Biological Perspective. *Protein Sci.* **2013**, *22* (2), 139−152.
(33) Kampes, R.; Zechel, S.; Hager, M. D.; Schubert, U. S. Halogen Bonding in Polymer Science: Towards New Smart Materials. *Chem. Sci.* **2021**, *12* (27), 9275−9286.
(34) Berger, G.; Soubhye, J.; Meyer, F. Halogen Bonding in Polymer Science: From Crystal Engineering to Functional Supramolecular Polymers and Materials. *Polym. Chem.* **2015**, *6* (19), 3559−3580.
(35) Puttreddy, R.; Jurcek, O.; Bhowmik, S.; Makela, T.; Rissanen, K. Very Strong $^-$N-X$^+\cdots{}^-$O-N$^+$ Halogen Bonds. *Chem. Commun.* **2016**, *52*, 2338.
(36) Perdew, J. P.; Ernzerhof, M.; Burke, K. Rationale for Mixing Exact Exchange with Density Functional Approximations. *J. Chem. Phys.* **1996**, *105* (22), 9982−9985.
(37) Perdew, J. P.; Burke, K.; Ernzerhof, M. Generalized Gradient Approximation Made Simple. *Phys. Rev. Lett.* **1996**, *77* (18), 3865−3868.
(38) Adamo, C.; Barone, V. Toward Reliable Density Functional Methods without Adjustable Parameters: The PBE0Model. *J. Chem. Phys.* **1999**, *110* (13), 6158−6170.
(39) Grimme, S.; Ehrlich, S.; Goerigk, L. Effect of the Damping Function in Dispersion Corrected Density Functional Theory. *J. Comput. Chem.* **2011**, *32* (7), 1456−1465.
(40) Grimme, S.; Antony, J.; Ehrlich, S.; Krieg, H. A Consistent and Accurate Ab Initio Parametrization of Density Functional Dispersion Correction (DFT-D) for the 94 Elements H-Pu. *J. Chem. Phys.* **2010**, *132* (15), 154104.
(41) Weigend, F.; Häser, M.; Patzelt, H.; Ahlrichs, R. RI-MP2: Optimized Auxiliary Basis Sets and Demonstration of Efficiency. *Chem. Phys. Lett.* **1998**, *294* (1), 143−152.
(42) Weigend, F.; Ahlrichs, R. Balanced Basis Sets of Split Valence, Triple Zeta Valence and Quadruple Zeta Valence Quality for H to Rn: Design and Assessment of Accuracy. *Phys. Chem. Chem. Phys.* **2005**, *7* (18), 3297−3305.
(43) Puttreddy, R.; Rautiainen, J. M.; Mäkelä, T.; Rissanen, K. Strong N−X···O−N Halogen Bonds: A Comprehensive Study on N-Halosaccharin Pyridine N-Oxide Complexes. *Angew. Chem., Int. Ed.* **2019**, *58* (51), 18610−18618.
(44) Parker, S. F.; Parker, J. L.; Jura, M. Structure and Vibrational Spectra of 2,5-Diiodothiophene: A Model for Polythiophene. *J. Phys. Chem. C* **2017**, *121* (23), 12636−12642.
(45) Bondi, A. Van Der Waals Volumes and Radii. *J. Phys. Chem.* **1964**, *68* (3), 441−451.
(46) Reichenbacher, K.; Suss, H. I.; Hulliger, J. Fluorine in Crystal Engineering-"the Little Atom That Could". *Chem. Soc. Rev.* **2005**, *34* (1), 22−30.
(47) Spackman, M. A.; Jayatilaka, D. Hirshfeld Surface Analysis. *CrystEngComm* **2009**, *11* (1), 19−32.
(48) McKinnon, J. J.; Jayatilaka, D.; Spackman, M. A. Towards Quantitative Analysis of Intermolecular Interactions with Hirshfeld Surfaces. *Chem. Commun.* **2007**, *37*, 3814−3816.
(49) Spackman, M. A.; McKinnon, J. J. Fingerprinting Intermolecular Interactions in Molecular Crystals. *CrystEngComm* **2002**, *4* (66), 378−392.
(50) Spackman, M. A.; McKinnon, J. J.; Jayatilaka, D. Electrostatic Potentials Mapped on Hirshfeld Surfaces Provide Direct Insight into Intermolecular Interactions in Crystals. *CrystEngComm* **2008**, *10* (4), 377−388.
(51) Yi, W.; Zhao, S.; Sun, H.; Kan, Y.; Shi, J.; Wan, S.; Li, C.; Wang, H. Isomers of Organic Semiconductors Based on Dithienothiophenes: The Effect of Sulphur Atoms Positions on the Intermolecular Interactions and Field-Effect Performances. *J. Mater. Chem. C* **2015**, *3* (41), 10856−10861.
(52) Liu, Y.; Di, C.; Du, C.; Liu, Y.; Lu, K.; Qiu, W.; Yu, G. Synthesis, Structures, and Properties of Fused Thiophenes for Organic Field-Effect Transistors. *Chem. − Eur. J.* **2010**, *16* (7), 2231−2239.
(53) Thordarson, P. Determining Association Constants from Titration Experiments in Supramolecular Chemistry. *Chem. Soc. Rev.* **2011**, *40* (3), 1305−1323.
(54) Rigaku. CrysAlisPro Software System. *Rigaku Oxford DIffraction 2017, Version 38.46*; Rigaku Corportation: Oxford, UK. 2017.
(55) Sheldrick, G. M. A Short History of SHELX. *Acta Crystallogr. A* **2008**, *64* (1), 112−122.
(56) Dolomanov, O. V.; Bourhis, L. J.; Gildea, R. J.; Howard, J. A. K.; Puschmann, H. OLEX2: A Complete Structure Solution, Refinement and Analysis Program. *J. Appl. Crystallogr.* **2009**, *42* (2), 339−341.
(57) Sheldrick, G. M. Crystal Structure Refinement with SHELXL. *Acta Crystallogr., Sect. C: Struct. Chem.* **2015**, *71* (1), 3−8.
(58) Nakajima, R.; Iida, H.; Hara, T. Synthesis and Spectral Properties of 5,5′-Di(4-Pyridyl)-2,2′-Bithienyl as a New Fluorescent Compound. *Bull. Chem. Soc. Jpn.* **1990**, *63* (2), 636−637.
(59) Abbotto, A.; Bradamante, S.; Facchetti, A.; Pagani, G. A.; K-y, A. *Introduction to Nonlinear Optical Effects in Molecules and Polymers*; Academic Press, 1997; Vol. *23*, pp 5755−5765.

https://doi.org/10.1021/acs.cgd.3c00958
Cryst. Growth Des. XXXX, XXX, XXX−XXX